The distribution of metals in cosmological hydrodynamical simulations of dwarf disc galaxies

K. Pilkington,[1,2,3]⋆ B. K. Gibson,[1,2,3] C. B. Brook,[1,4] F. Calura,[1,5] G. S. Stinson,[1,6]
R. J. Thacker,[2] L. Michel-Dansac,[7] J. Bailin,[8] H. M. P. Couchman,[9] J. Wadsley,[9]
T. R. Quinn[10] and A. Maccio[6]

[1]*Jeremiah Horrocks Institute, University of Central Lancashire, Preston PR1 2HE*
[2]*Department of Astronomy & Physics, Saint Mary's University, Halifax, Nova Scotia, B3H 3C3, Canada*
[3]*Monash Centre for Astrophysics, School of Mathematical Sciences, Monash University, Clayton, VIC, 3800, Australia*
[4]*Departamento de Física Teórica, Universidad Autónoma de Madrid, E-28049 Cantoblanco, Madrid, Spain*
[5]*Istituto Nazionale di Astrofisica, Osservatorio Astronomico di Bologna, Via Ranzani 1, I-40127, Bologna, Italy*
[6]*Max-Planck-Institut für Astronomie, Königstuhl 17, 69117 Heidelberg, Germany*
[7]*Centre de Recherche Astrophysique de Lyon, Université de Lyon, Obs. de Lyon, CNRS, Saint-Genis Laval, 69230, France*
[8]*Astronomy Department, University of Michigan, 500 Church Street, Ann Arbor, MI 48109-1042, USA*
[9]*Department of Physics & Astronomy, McMaster University, Hamilton, Ontario, L8S 4M1, Canada*
[10]*Astronomy Department, University of Washington, Box 351580, Seattle, WA 98195, USA*

ABSTRACT

We examine the chemical properties of five cosmological hydrodynamical simulations of an M33-like disc galaxy which have been shown previously to be consistent with the morphological characteristics and bulk scaling relations expected of late-type spirals. These simulations are part of the Making Galaxies in a Cosmological Context Project, in which stellar feedback is tuned to match the stellar mass–halo mass relationship. Each realization employed identical initial conditions and assembly histories, but differed from one another in their underlying baryonic physics prescriptions, including (a) the efficiency with which each supernova energy couples to the surrounding interstellar medium, (b) the impact of feedback associated with massive star radiation pressure, (c) the role of the minimum shut-off time for radiative cooling of Type II supernovae remnants, (d) the treatment of metal diffusion and (e) varying the initial mass function. Our analysis focusses on the resulting stellar metallicity distribution functions (MDFs) in each simulated (analogous) 'solar neighbourhood' (2–3 disc scalelengths from the galactic centre) and central 'bulge' region. We compare and contrast the simulated MDFs' skewness, kurtosis and dispersion (inter-quartile, inter-decile, inter-centile and inter-tenth-percentile regions) with that of the empirical solar neighbourhood MDF and Local Group dwarf galaxies. We find that the MDFs of the simulated discs are more negatively skewed, with higher kurtosis, than those observed locally in the Milky Way and Local Group dwarfs. We can trace this difference to the simulations' very tight and correlated age–metallicity relations (compared with that of the Milky Way's solar neighbourhood), suggesting that these relations within 'dwarf' discs might be steeper than in $L_\star$ discs (consistent with the simulations' star formation histories and extant empirical data), and/or the degree of stellar orbital redistribution and migration inferred locally has not been captured in their entirety, at the resolution of our simulations. The important role of metal diffusion in ameliorating the overproduction of extremely metal-poor stars is highlighted.

Key words: methods: numerical – galaxies: abundances –galaxies: evolution.

⋆E-mail: kpilkington@uclan.ac.uk

1 INTRODUCTION

The relative number of stars of a given metallicity in a given environment, whether it be the local stellar disc, central spheroid/bulge and/or baryonic halo – the so-called metallicity distribution function (MDF) – has embedded within it the time evolution of a system's star formation, assembly/infall and outflow history, all convolved with the initial mass function (IMF; Tinsley 1980). Seminal reviews of the diagnostic power of the MDF include those of Haywood (2001) and Caimmi (2008).

Well in advance of our now empirical appreciation of (a) the hierarchical assembly of galaxies from sub-galactic units, (b) the ongoing infall of fresh material from haloes to discs (e.g. high-velocity clouds; Gibson et al. 2001) and (c) the ongoing outflow of enriched material from discs via stellar- and supernovae (SNe)-driven winds/fountains (e.g. McClure-Griffiths et al. 2006), it was recognized that the local MDF provided crucial evidence that the Milky Way (and presumably galaxies as a whole) did not behave as a 'closed-box' in an evolutionary sense (Pagel & Patchett 1975).

This latter recognition was perhaps best manifest in what became known as the 'G-dwarf problem' (Hartwick 1976); specifically, a simple model in which gas was not allowed to infall or outflow from the system would necessarily lead to a significant population of long-lived, low-metallicity stars in the solar neighbourhood, with ~ 20 per cent of the stars locally predicted to possess metallicities below $[Fe/H] \approx -1$ (Tinsley 1980). In nature, such a population is not observed, with the empirical fraction of local low-metallicity stars being approximately two orders of magnitude smaller than the aforementioned closed-box predictions (e.g. Kotoneva et al. 2002; Casagrande et al. 2011).

Since this recognition of its fundamental importance, the MDF has acted as one of the primary constraints/boundary conditions against which all analytical (e.g. Schörck et al. 2009; Kirby et al. 2011), seminumerical (e.g. Chiappini, Matteucci & Romano 2001; Fenner & Gibson 2003) and chemo-dynamical (e.g. Roškar et al. 2008; Sánchez-Blázquez et al. 2009; Tissera, White & Scannapieco 2011; Calura et al. 2012) models are compared.

From a chemo-dynamical perspective, recent work has focused on the sensitivity of global metal redistribution to different physical prescriptions within the context of the OWLS project (Wiersma, Schaye & Theuns 2011); at higher redshift, a similar, equally comprehensive, study was undertaken by Sommer-Larsen & Fynbo (2008). In both cases, the emphasis was placed on the whereabouts of the 'missing metals' – i.e. metals thought to reside in the warm-hot intergalactic medium and/or haloes of massive galaxies, but have thus far proven challenging to detect directly.[1] While not fully cosmological, the reader is also referred to the chemo-dynamical work of Kobayashi & Nakasato (2011) for a complementary analysis of a simulated Milky Way-like system.

Each of the above chemo-dynamical studies examines cursory aspects of the MDF 'constraint', but the focus for each was never meant to be a comprehensive analysis of the dispersion and higher order moments of the shape characteristics,[2] nor their link to the associated age–metallicity relations (AMRs), star formation histories (SFHs) and putative G-dwarf problem; such higher order

moments include the MDF skewness, kurtosis, and inter-quartile (IQRs), inter-decile (IDRs), inter-centile (ICRs) and inter-tenth-percentile regions (ITPRs).

The skewness of an MDF can be a reflection of both the classical G-dwarf problem and the slope of the AMR; kurtosis is often thought of as being a measure of the 'peakedness' of the MDF (e.g. by how much the peak is 'flatter' or 'peakier' than a Gaussian), while in practice it is often more sensitive to the presence of 'heavy' tails, rather than the shape of the peak; the IQRs, IDRs, etc. probe both the effects of SFHs and AMRs and, in the case of the ICRs and (especially) the ITPRs, the impact of metal diffusion on the extreme metal-poor tail of the distribution. In the context of cosmological chemo-dynamical disc simulations, to our knowledge, our's is the first quantitative discussion of these higher order moments of the MDF.

Further, from an observational perspective, the recent recalibrations of the original Geneva–Copenhagen Survey (GCS; Nordström et al. 2004) by Holmberg, Nordström & Andersen (2009) and Casagrande et al. (2011) has made for a timely investigation of the predicted characteristics of the MDFs of simulated disc galaxies. Parallel developments slightly further afield[3] include targeted MDF studies of the thin–thick disc transition region and the thick disc proper (Schlesinger et al. 2012), the stellar halo (Schörck et al. 2009) and the Galactic bulge (Bensby et al. 2011; Hill et al. 2011).

This paper aims to fill a gap in the literature, by making use of a new suite of fully cosmological chemo-dynamical simulations whose properties have been shown to be in remarkable agreement with the basic scaling laws to which late-type disc galaxies adhere in nature (Brook et al. 2012b; Macciò et al. 2012). The simulations themselves are outlined briefly in Section 2, alongside a description of the adopted analogous 'solar neighbourhood' regions. The associated AMRs are presented in Section 3; the need for this will become apparent when analysing the higher order moments of the MDFs within these regions and, in particular, their metal-poor tails (Section 4). Our results will then be summarized in Section 5.

2 SIMULATIONS

In what follows, we analyse five cosmological zoom variants of the 'scaled-down' M33-like disc galaxy simulation (g15784) described by Brook et al. (2012a). The initial conditions are identical for each realization, and taken from the eponymous g15784 of Stinson et al. (2010) after rescaling (e.g. Kannan et al. 2012) the mass (length) scales by a factor of 8 (2). Differences in the underlying power spectrum that result from this rescaling are minor (e.g. Springel et al. 2008; Kannan et al. 2012; Macciò et al. 2012; Vera-Ciro et al. 2012), and do not affect our results. The virial mass of the scaled g15784 is 2×10^{11} M$_\odot$, with $\sim 10^7$ particles within the virial radius at $z = 0$, with a mean stellar particle mass of ~ 6400 M$_\odot$. A gravitational softening of $\epsilon = 155$ pc was used; to ensure that gas resolves the Jeans mass, rather than undergoing artificial fragmentation, pressure is added to the gas, after Robertson & Kravtsov (2008). Further, a maximum density limit is imposed by setting the minimum smoothed particle hydrodynamics (SPH) smoothing length to be 1/4 that of the softening length.[4]

---

[1] Tumlinson et al. (2011) is an example of recent efforts, though, to characterize the properties of these difficult-to-observe baryon reservoirs.

[2] cf. Kirby et al. (2011), though, for a study of the higher order moments of the MDFs of Local Group dwarf spheroidals, which is similar in spirit to our work here on disc galaxies.

[3] Spatially speaking, in relation to that of the solar neighbourhood region probed by the GCS.

[4] In comparison, the original Stinson et al. (2010) simulations used a minimum SPH smoothing length of $\epsilon/100$, resulting a dramatic increase in computational time, but with only minimal impact on the simulation itself.

Table 1. Primary parameters employed for the five simulations analysed in this work. Column 1: simulation/galaxy name; column 2: adopted IMF (Kroupa≡Kroupa et al. 1993; Chabrier≡Chabrier 2003); column 3: star formation efficiency; column 4: thermalized SN energy fraction coupled to the ISM; column 5: thermalized massive star radiation energy fraction coupled to the ISM; column 6: maximum allowable gas temperature for star formation; column 7: present-day stellar mass (in solar masses) within the virial radius; column 8: stellar disc exponential scalelength (in kpc); column 9: vertical [Fe/H] gradient (in dex kpc^{-1}); column 10: radial [Fe/H] gradient (in dex kpc^{-1}).

Galaxy	IMF	$c_\star$	ϵSN (per cent)	SR (per cent)	T_{max} (K)	Stellar mass ($M_\odot$)	Scalelength (kpc)	Vertical gradient (dex kpc^{-1})	Radial gradient (dex kpc^{-1})
11mKroupa	Kroupa	0.1	100	10	15 000	7.1×10^9	2.34	−0.064	−0.012
11mChab	Chabrier	0.075	100	10	10 000	1.3×10^9	2.78	−0.017	−0.026
11mNoRad	Kroupa	0.1	100	0	15 000	9.1×10^9	1.58	−0.027	−0.045
11mNoMinShut	Kroupa	0.1	100	10	15 000	14.0×10^9	1.71	−0.008	−0.020
11mNoDiff	Kroupa	0.1	100	10	10 000	2.1×10^9	1.43	−0.013	−0.028

Each of the five simulations was evolved using the gravitational *N*-body + SPH code GASOLINE (Wadsley, Stadel & Quinn 2004). Metal-dependent cooling of the gas, under the assumption of ionization equilibrium, is applied, after Shen, Wadsley & Stinson (2010), coupled to a uniform, evolving, Haardt & Madau (1996) ionizing ultraviolet background. Our reference/fiducial simulation (11mKroupa) was introduced by Brook et al. (2012a), in the context of its outflow and angular momentum characteristics. The structural and kinematic properties (e.g. rotation curves, bulge-to-disc decomposition, ratio of rotational-to-anisotropic support, etc.) of the simulations presented here are indistinguishable from those presented in Brook et al. (2012a), to which the reader is referred for supplementary details.

When gas reaches a sufficiently cool temperature ($T < 10\,000$–$15\,000$ K) and resides within a sufficiently dense environment ($n_{th} > 9.3$ cm^{-3}),[5] it becomes eligible to form stars according to $\frac{dM_\star}{dt} = c_\star \frac{M_{gas}}{t_{dyn}}$, where $c_\star$ is the star formation efficiency,[6] Δt is the timestep between star formation events (0.8 Myr, here), M_{gas} is the SPH particle mass, t_{dyn} is the SPH particle's dynamical time and $\Delta M_\star$ is the mass of the star particle formed.

We have extended the chemical 'network' of GASOLINE from oxygen and iron, to now also track the evolution of carbon, nitrogen, neon, magnesium and silicon. After Raiteri, Villata & Navarro (1996), power-law fits to the Woosley & Weaver (1995) $Z = 0.02$ Type II SNe yields were generated for the dominant isotopes for each of these seven elements; a further extension was implemented, in order to include the van den Hoek & Groenewegen (1997) metallicity-dependent carbon, nitrogen and oxygen yields from asymptotic giant branch stars. By expanding upon the chemical species being tracked, the earlier concern regarding the underprediction of the global metallicity by a factor of ∼2 (and the consequent underestimate to the SPH cooling and star formation rates) is naturally alleviated (Pilkington et al. 2012b). We note in passing that all abundances (and ratios) presented here are relative to the solar scale defined by Asplund et al. (2009).

Feedback from SNe follows the blastwave formalism of Stinson et al. (2006), with 100 per cent of the energy (10^{51} erg/SN) thermally coupled to the surrounding interstellar medium (ISM). Cooling is disabled for particles within the blast region (corresponding to the radius of the remnant when the interior pressure has been reduced to that of the pressure of the ambient ISM) for a time-scale corresponding to that required to cool the hot interior gas to $T \sim 10^4$ K.[7] Bearing in mind the 0.8 Myr timesteps of our runs, we impose a minimum cooling 'shut-off time' which matches this value.[8]

We employ the Making Galaxies in a Cosmological Context feedback model described by Brook et al. (2012a) and Stinson et al. (2012), taking into account the effect of energy feedback from massive stars into the ISM[9] (cf. Hopkins, Quataert & Murray 2011). While a typical massive star might emit ∼10^{53} erg of radiation energy during its pre-SN lifetime, these photons do not couple efficiently to the surrounding ISM; as such, we only inject 10 per cent of this energy in the form of thermal energy into the surrounding gas, and cooling is not disabled for this form of energy input. Of this injected energy, typically 90–100 per cent is radiated away within a single dynamical time.

The default IMF is that of Kroupa, Tout & Gilmore (1993); the 11mChab run incorporates the more contemporary (and currently favoured) Chabrier (2003) functional form; as per stellar generation, the latter possesses a factor of ∼4 times the number of Type II SNe as that of the former. Finally, the treatment of metal diffusion within GASOLINE is detailed by Shen et al. (2010); a diffusion coefficient $C = 0.05$ has been adopted for our runs, except for one simulation for which diffusion was prohibited (11mNoDiff).[10] The primary numerical characteristics of the five simulations employed here are listed in Table 1.

For our MDF and AMR analyses, for each simulation, we identify an analogous region to that of the Milky Way's 'solar neighbourhood', defined to be a radial range from 3.0 to 3.5 disc scalelengths (see Table 1) and to lie within 500 pc of the galactic midplane. The fraction of accreted stars in these high-feedback runs is negligible; as such their contamination in the 'solar neighbourhood' is equally negligible. Consequently, there was no need to undertake the sort of kinematic decomposition of the orbital circularity $\epsilon_J \equiv J_z/J_{circ}(E)$ distribution[11] that was needed to isolate

---

[5] The star formation density threshold n_{th} corresponds to the maximum density gas can reach using gravity – i.e. $n_{th} = 32M_{gas}/\epsilon^3$.

[6] The star formation efficiency $c_\star$ was taken to be 10 per cent for all the runs, except for 11mChab, for which a value of 7.5 per cent was adopted.

[7] To use the terminology of Gibson (1994), the relevant radius and time-scale correspond to R_{merge} and t_{cool}, respectively.

[8] Save, for the one run for which this restriction was relaxed (11mNoMinShut).

[9] Except for the one run included here without radiation energy (11mNoRad).

[10] Our 'no diffusion' run possesses MDF and chemical 'characteristics' similar to those of DG1 (Governato et al. 2010); a brief chemical analysis for the latter was shown in Pilkington et al. (2012a). This similarity can be traced to the less efficient metal diffusion adopted for the DG1 runs (i.e. $C = 0.01$ versus the $C = 0.05$ now employed for our GASOLINE runs, after Shen et al. 2010).

[11] Where J_z is the *z*-component of the specific angular momentum and $J_{circ}(E)$ is the angular momentum of a circular orbit at a given specific binding energy.
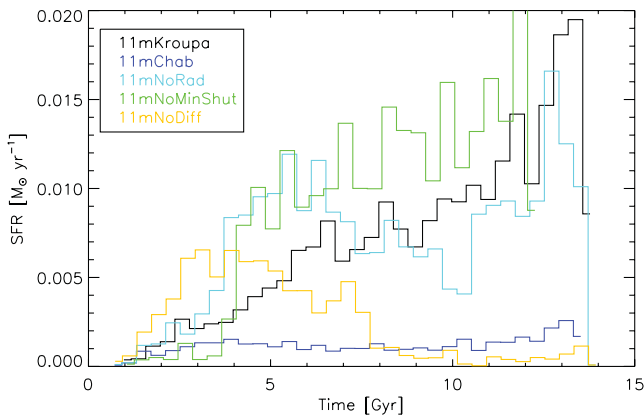
Figure 1. SFHs of the solar neighbourhoods associated with the five simulations; colour coding is as noted in the inset to the panel.

disc/in situ stars from spheroid/accreted stars in our parallel analysis of the MDFs of the more massive (and accretion-contaminated) Stinson et al. (2010) simulations (Calura et al. 2012).[12]

We first show the inferred SFHs of the solar neighbourhoods associated with each of the five simulations (Fig. 1). Several important points should be made before analysing the AMRs and MDFs. Qualitatively speaking, the SFHs of these regions within `11mKroupa`, `11mNoMinShut` and `11mNoRad` are similar to those seen in gas-rich dwarfs like NGC 6822, Sextans A, WLM, and to some extent, the Large Magellanic Cloud (LMC; Dolphin et al. 2005). In that sense, they are (not surprisingly) different from the typical exponentially decaying SFH (time-scales of $\sim5-7$ Gyr) inferred for the Milky Way's solar neighbourhood (e.g. Renda et al. 2005), and so we should not expect *identical* trends in the ancillary AMRs and MDFs, as those observed locally. Indeed, we will show this to be case momentarily, but our interest here is more in identifying trends, rather than *exact* star-by-star comparisons.

The one simulation which shows an exponentially declining SFH at later times is that of `11mNoDiff`; the lack of diffusion here acts to minimize the 'spread' of metals to a degree that star formation is restricted (preferentially) to much less enriched SPH particles (in part), because the cooling then becomes less efficient for a greater number of SPH particles, which has a greater impact at later times where there are fewer efficiently cooling metal-enriched SPH particles out of which to potentially form stars. We will return to the special case of the 'no diffusion' model shortly.

The SFH of `11mChab` also shows a distinct behaviour relative to the `11mKroupa` fiducial. Specifically, it is significantly lower, and relatively constant, at all times; in spirit, this is similar to the inferred SFH of the LMC (e.g. Holtzman et al. 1999). This is reflected in the stellar mass at $z = 0$ being significantly lower than `11mKroupa`, which in turn aids considerably in bringing its properties into close

[12] Note that this was confirmed by undertaking a kinematic decomposition of `11mKroupa` using the modified technique introduced by Abadi et al. (2003), and employed by Calura et al. (2012); specifically, none of our conclusions were contingent upon the need for a kinematic decomposition. More quantitatively, only ~3 per cent of the stars in our simulated 'solar neighbourhoods' would be kinematically classified as 'bulge/spheroid' stars, impacting on the various MDF metrics to be discussed later at the <3 per cent level [smaller than the uncertainty associated with the treatment of extreme ($>5\sigma$) outliers – see Section 4]. In light of this negligible impact, we have avoided imposing any personal preferred kinematic decomposition scheme into the analysis.

agreement with essentially all traditional scaling relations (Brook et al. 2012b). This behaviour is driven by (a) the factor of 4 increase in the SNe per stellar generation (via the more massive star-biased IMF) and (b) the reduced maximum temperature for star formation (as noted earlier).

The subtle effect of allowing the minimum shut-off time for radiative cooling of SN remnants to become prohibitively small in high-density regions (in practice what this means is that the shut-off time becomes smaller than the timestep of 0.8 Myr) can be seen in the `11mNoMinShut` curve of Fig. 1. Specifically, SPH particles affected by this effectively cool 'instantly' within the same timestep, without any delay. Hence, the particles in question become 'available' for star formation much sooner than they might otherwise; this has the effect of 'boosting' the star formation relative to that of the fiducial `11mKroupa`.

3 AGE–METALLICITY RELATIONS

As noted earlier, the MDF bears the imprint of a region's SFH, convolved with its AMR. Having introduced the 'solar neighbourhood' SFHs in Section 2, we now present their associated AMRs in Fig. 2. The time evolution of the [Fe/H] abundances is shown for each of the five simulations listed in Table 1. Colour coding within each panel corresponds to stellar age, ranging from old (black/blue) to young (red).

To provide a representative empirical data set against which to compare, we make use of the recent recalibration of the GCS presented by Holmberg et al. (2009). The base GCS provides invaluable spectral parameters for $\sim17\,000$ F- and G-type stars in the solar neighbourhood. Following Holmberg, Nordström & Andersen (2007), we define a 'cleaned' subsample by eliminating (i) binary stars, (ii) stars for which the uncertainty in age is >25 per cent, (iii) stars for which the uncertainty in trigonometric parallax is >13 per cent and (iv) stars for which a 'null' entry was
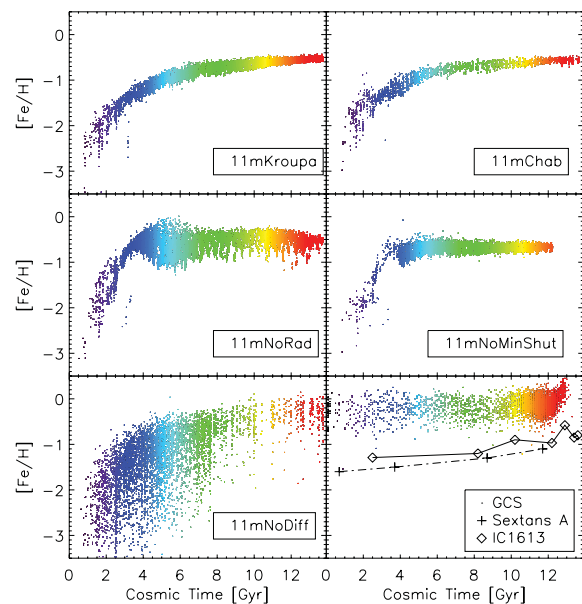

Figure 2. AMRs (where metallicity $\equiv$ [Fe/H]) in the analogous solar neighbourhoods of the five simulations employed here, in addition to the reference relationship found in the solar neighbourhood of the Milky Way, and the dwarf irregulars Sextans A (Dolphin et al. 2003) and IC 1613 (Skillman et al. 2003). Colour coding in each panel is by stellar age, ranging from black/blue (oldest) to red (youngest).

provided for any of the parallax, age, metallicity or their associated uncertainties. The AMR for this 'cleaned' subsample of ∼4000 stars is shown in the lower-right panel of Fig. 2. A fifth criterion is applied for the determination of the higher order moments of the MDF shape; specifically, following Holmberg et al. (2007) and constructing an unbiased volume-limited subsample from the stars lying within 40 pc of the Sun. Doing so yields a smaller sample of only ∼500 stars. While this does not impact on the shape characteristics of Section 4 or the behaviour of the AMR, for clarity, we show the AMR inferred from the aforementioned subsample of ∼4000 stars in Fig. 2.[13]

It is worth re-emphasizing that we are using the Holmberg et al. (2009) variant of the GCS solely as a useful 'comparator' against which to contrast our various MDF metrics/higher order moments. It should not be interpreted as an endorsement of one solar neighbourhood MDF over another; there is a rich literature describing the various pros and cons of any number of potential selection biases within this (or any other) recalibration of the GCS (e.g. Schoenrich & Binney 2008; Casagrande et al. 2011) and we are not equipped to enter into that particular debate. The GCS remains the standard bearer for MDF analysis, reflecting the nature of (fairly) volume-limited and (fairly) complete nature, making it ideal for probing the active star-forming component of the thin disc; other exquisite MDFs, including those of the aforementioned (predominantly) thick disc (Schlesinger et al. 2012) and halo (Schörck et al. 2009) studies, are more suited for simulations targeting regions further from the mid-plane than we are doing here. Ideally, of course, we would like to replace the solar neighbourhood 'comparator' used here (the GCS) with an empirical sample more representative of SFHs associated with massive dwarf spiral/irregulars (e.g. Dolphin et al. 2003; Skillman et al. 2003; Kirby et al. 2011), but until the statistics, completeness and accuracy of the age and metallicity determinations for such distance dwarfs reach that of the solar neighbourhood, we are reluctant to compare (in detail) the predictions of the simulations with those of the observations. Having said that, we will comment on, in a qualitative sense, the AMR and MDF trends seen in our simulations and how they compare with said dwarfs.

Several key points can be inferred from Fig. 2. First, not surprisingly, the metallicities of the stars in the Milky Way's solar neighbourhood (GCS) are typically a factor of ∼5–100 times higher at a given age compared with the five simulations. This reflects the discussion of Section 2 in relation to the fact that the simulations in question are more similar to lower luminosity disc galaxies (in terms of both mass and SFHs), rather than being Milky Way 'clones'. Secondly, the simulations are consistent with the various scaling relations to which galaxies adhere (Brook et al. 2012b); as such, for their mass, their mean metallicities are a factor of ∼3–5 times lower than that of the Milky Way.[14]

More important for our purposes here are two additional characteristics which are readily apparent in Fig. 2. First, the AMR of the

solar neighbourhood is essentially non-existent, save for a trace of old, metal-poor stars. In contrast, the corresponding regions of the simulations show *extremely* correlated AMRs (especially those of the fiducial simulations, 11mKroupa and 11mChab). This is partly traced to the differences in the aforementioned SFHs, although the correlation persists (admittedly with larger scatter at a given age) even in 11mNoDiff, the simulation whose SFH bears the closest resemblance to that of the Milky Way. The impact of these tightly correlated AMRs manifest themselves significantly within the inferred MDFs, a point to which we will return in Section 4. Qualitatively speaking, these tightly correlated AMRs resemble those predicted by seminumerical galactic chemical evolution models (e.g. Chiappini et al. 2001; Fenner & Gibson 2003; Mollá & Díaz 2005; Renda et al. 2005).

In the bottom-right panel of Fig. 2, we also overplot the AMRs inferred from the colour–magnitude diagram-derived SFHs of the dwarf irregulars Sextans A (Dolphin et al. 2003) and IC 1613 (Skillman et al. 2003); like the Milky Way, neither are meant to be one-to-one matches to the 11m series of simulations, but in some sense they do provide a useful complementary constraint, in the sense that their respective SFHs are not dissimilar to those shown in Fig. 1 (in particular, those of 11mKroupa, 11mNoMinShut and 11mNoRad). Their associated AMRs, while lacking the statistics, completeness and accuracy of the GCS data set necessary to make detailed quantitative comparisons, do show evidence of possessing somewhat stronger correlations. Again, the statistics of these dwarf systems' MDFs and AMRs make it difficult to say anything more regarding the degree of 'agreement' between the 11m series and that encountered in nature, but it is suggestive and certainly merits revisiting once data comparable to that of the GCS becomes available for dwarf irregulars/spirals.

Secondly, the scatter in [Fe/H] at a given stellar age is significantly smaller (compared with that of the Milky Way) in the three simulations where the injection of thermalized massive star radiation energy to the surrounding ISM is included (i.e. 11mKroupa, 11mChab and 11mNoMinShut). Neglecting this feedback term, within the context of these cosmological hydrodynamical disc simulations, acts to increase the scatter in [Fe/H], at a given in time, to a level comparable to that seen in Milky Way's solar neighbourhood.[15] Not surprisingly, the one simulation for which metal diffusion was suppressed (11mNoDiff) possesses the largest scatter in [Fe/H] at a given age, particularly at early times/low metallicities, where the neglect of diffusion is most problematic (again, a point to which we return in Section 4).

4 METALLICITY DISTRIBUTION FUNCTIONS

Having been informed by the empirical and simulated solar neighbourhoods' SFHs and AMRs (Sections 2 and 3, respectively), we now present the [Fe/H] MDFs for the same regions.[16] Fig. 3 shows the MDFs (black histograms) for the five simulations, the Milky Way (GCS: lower-right panel) and the Local Group dwarf Fornax (also, lower-right panel, from Kirby et al. 2011). The two subsamples of the GCS are shown: in black, the aforementioned (Section 3)

---

[13] The 'upturn' towards high metallicities at young ages in the GCS sample is likely traced to the very young Fm/Fp stars which are difficult to characterize with Stromgren photometry alone (Holmberg et al. 2009).

[14] The MDFs and AMRs of systems more directly comparable to the Milky Way proper – i.e. the more massive 'parent' simulations to those employed here (Stinson et al. 2010) – are described by Calura et al. (2012) and Bailin et al. (in preparation), respectively. The significant contamination from accreted stars in these more massive simulations tends to impact upon both the scatter of the AMR and skewness/dispersion of the IMF, in a negative sense, relative to the high-feedback models here, for which the accreted fraction is negligible.

[15] A secondary byproduct is also a mildly steeper radial abundance gradient, although the effect is minor – recall Table 1.

[16] We confirmed that our conclusions are robust to the specific definition of the 'solar neighbourhood', by increasing its vertical range from ±0.5 to ±2 kpc. Similarly, varying the radial range from 3.50 ± 0.25 disc scalelengths by ±1 scalelength has negligible impact (recall from Table 1 that the metallicity gradients here are shallow).
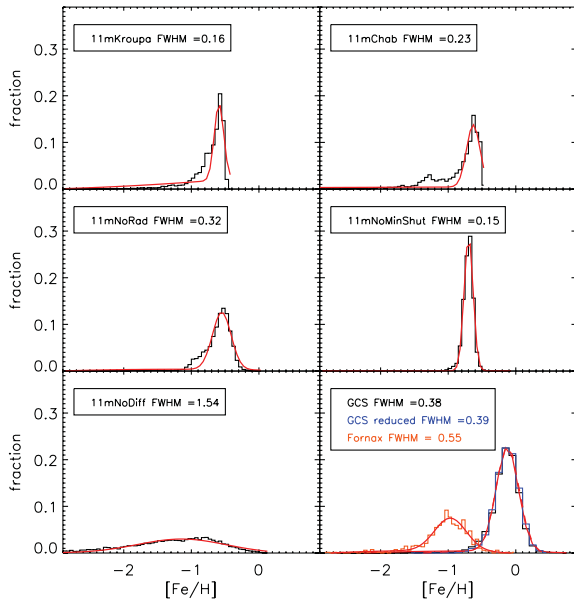
Figure 3. The [Fe/H] MDFs in the solar neighbourhoods of the five simulations employed here. The bottom-right panel shows the MDF of the Milky Way's solar neighbourhood, based upon two subsamples of stars selected from Holmberg et al. (2009), as well as that for Local Group dwarf Fornax, from Kirby et al. (2011) (see the text for details). In each panel, the overlaid curve is the best-fitting single component Gaussian to the aforementioned MDF; the associated FWHM of said Gaussian is listed in the inset to each panel.

subsample of ∼4000 stars (matching those shown in Fig. 2 – i.e. the 'cleaned' subsample, but without any distance constraint applied, labelled 'GCS' in the lower-right panel), and in blue, the volume-limited sample (i.e. those lying within 40 pc of the Sun, labelled 'GCScut'). As stressed earlier, the shape characteristics of the GCS MDF are not contingent upon this latter cut; the labels 'GCS' and 'GCScut' will be employed to differentiate between the two, where relevant. Overlaid in each panel is simple 'best-fitting' (single) Gaussian to the respective distributions [and their associated full width at half-maximum (FWHM) values]. For the Fornax dwarf, we use the full sample of 675 stars taken from Kirby et al. (2011), in order to show an MDF for a representative local dwarf. Three caveats should be noted, in relation to the latter: (i) the sample size is one to two orders of magnitude smaller than the GCS, not surprisingly, considering the challenging nature of this observational work; (ii) no analogous 'solar neighbourhood' can be identified within this data set (it is simply all the stars in the sample covering a range of fields in Fornax) and (iii) the uncertainty in [Fe/H] for a given individual star in Fornax is ∼0.5 dex, compared with the ∼0.1 dex associated with individual stars in the GCS. Fornax is neither better nor worse than the GCS, as a comparator, so it is useful to at least show both, as they represent the state of the art, observationally speaking.

Even before undertaking any quantitative analysis of the MDFs, it is readily apparent that the simulations (particularly, 11mKroupa and 11mChab) possess an excess of stars to the left (i.e. to the negative side) of the peak of the MDF, relative to the right, when compared with that of the GCS and Fornax (i.e. the simulated MDFs are more negatively skewed). This 'excess' of lower metallicity stars are formed in situ during the first ∼4 Gyr of the simulations. The exception to this trend is 11mNoMinShut, for which the lack of significant star formation at early epochs (recall Fig. 1) and the

extremely flat AMR at late times (Fig. 2) conspires to present the narrow and symmetric MDF shown in Fig. 3. As noted in Section 3, for both 11mNoRad and 11mNoDiff, the larger scatter in [Fe/H] at a given age manifests itself in the broader MDFs seen in Fig. 3.

It is worth delving deeper into the source of the broader MDF seen in, for example, 11mNoRad, relative to the fiducial 11mKroupa. Here, it is at high redshift that the radiation energy has an impact on the regulation of star formation. 11mNoRad has higher star formation at early times (Fig. 1), but not at later times, primarily because it exhausts its available gas, whereas with the radiation energy star formation is regulated during that crucial period when gas accretion is most active; this gas remains available at later times to form stars, resulting in the MDF of 11mNoRad being broader relative to the fiducial. Ultimately, the length of time that gas spends in the disc before it forms stars shapes the MDF 'width' here. With radiation energy included, this gas is in the disc for a longer period of time, meaning more metal mixing occurs. Linking back to the SFHs of Fig. 1, we note that most of the gas is accreted during the first ∼6 Gyr, and one can see that the star formation rate shows that early peak in the case of 11mNoRad (and 11mNoDiff), but not in the cases which include radiation energy – i.e. gas that forms stars (relatively) rapidly after accretion does not mix as much, and hence the broader MDF.

We next undertook a quantitative analysis of the MDFs shown in Fig. 3, including a determination of the skewness, kurtosis and widths in a range of inter-percentiles of the distributions. These determinations are listed in Table 2. As both skewness and kurtosis are highly sensitive to the presence of outliers, we imposed a fairly standard 5σ clipping to the distributions. To mimic the observational uncertainties associated with the determination of individual stellar [Fe/H] abundances, after Fenner & Gibson (2003), the 'theoretical' MDFs shown in Fig. 3 were convolved first with either a 0.1 dex Gaussian (to mimic the GCS uncertainties – Holmberg et al. 2009) or a 0.5 dex Gaussian (to mimic the uncertainties with the Fornax data – Kirby et al. 2011). In Table 2, each column has two numbers; the first is the relevant metric, as measured on the MDF convolved with a 0.1 dex Gaussian, while the second (in parentheses) is that measured on the MDF convolved with a 0.5 dex Gaussian. As the simulated MDFs are typically much broader than the GCS uncertainties, the impact of the 0.1 dex smoothing is minimal.

As inferred from the above qualitative discussions of the MDF and AMR (Section 3), MDFs of the simulated solar neighbourhoods are all (save for 11mNoMinShut, whose exceedingly flat AMR results in the elimination of essentially all tails, positive or negative of the MDF's peak) more negatively skewed than that of the Milky Way's solar neighbourhood (from both the volume-limited GCScut sample of stars and the unrestricted GCS sample) and the sample from Fornax. It must be emphasized though that the typical 0.5 dex uncertainty associated with the determination of [Fe/H] for individual stars in Fornax means that broadening the simulated MDFs, with their typical dispersions of ∼0.1 dex, by 0.5 dex, 'washes out' much of our ability to compare and contrast the higher order MDF metrics, and hence the analysis which follows emphasizes the differences between the simulated MDFs and that of the GCS. The 'tail' of stars to the negative side of the peak should not be associated immediately with the traditional 'G-dwarf problem', since these fully cosmological simulations relax the 'closed-box' framework which is the hallmark of this problem. Instead, as noted earlier, it is the tightly correlated AMRs which are driving the large negative skewness values; these AMRs do not resemble that of the Milky Way's solar neighbourhood. The different SFHs are certainly part of the difference, but as noted earlier, both the fiducial 11mChab

Table 2. Primary MDF shape characteristics for the solar neighbourhoods of the five simulations described here; the two subsamples based upon the Holmberg et al. (2009) GCS empirical data set are as described in the text and data for the Fornax dwarf galaxy taken from Kirby et al. (2011). After Fenner & Gibson (2003), the simulated MDFs were convolved with either a 0.1 dex Gaussian (leftmost entry within each column) or a 0.5 dex Gaussian (rightmost/bracketed entry within each column) to mimic the typical uncertainties associated with the [Fe/H] determinations in nature (the GCS in the case of the former and Fornax in the case of the latter). Column 1: the name of the simulation or empirical data set; column 2: the skewness of the MDF (5σ clipping of outliers was imposed, to minimize their impact on the determination); column 3: the kurtosis of the MDF, again with the adoption of 5σ clipping; columns 4–7: the inter-quartile (IQR), inter-decile (IDR), inter-centile (ICR) and inter-tenth-percentile (ITPR) region for each MDF.

Simulation/Data set	Skewness	Kurtosis	IQR	IDR	ICR	ITPR
11mKroupa	−1.84(−1.21)	3.83(2.59)	0.30(0.54)	0.67(1.13)	1.59(2.72)	2.49(4.34)
11mChab	−1.56(−1.15)	2.43(2.37)	0.41(0.60)	0.85(1.28)	1.71(2.96)	2.38(5.04)
11mNoRad	−1.13(−0.93)	2.45(1.88)	0.26(0.47)	0.52(0.92)	1.44(2.07)	2.39(3.73)
11mNoMinShut	+0.47(−0.29)	0.94(0.57)	0.13(0.48)	0.26(0.93)	0.69(1.79)	1.97(3.26)
11mNoDiff	−0.91(−1.29)	0.91(2.32)	0.96(1.25)	1.85(2.44)	3.49(5.18)	5.06(8.03)
GCS	−0.61	2.04	0.23	0.48	1.26	2.63
GCScut	−0.37	0.78	0.24	0.45	0.94	1.43
Fornax	(−1.33)	(3.58)	(0.38)	(2.25)	(2.75)	(2.85)

and 11mNoDiff show SFHs not dissimilar to the exponentially declining one of the Milky Way, and the coordinated AMRs remain responsible for the larger negative skewness in both cases. An analysis of the kurtosis values for each distribution is consistent with this picture. Specifically, the simulations' kurtosis values are all larger than those of GCScut, and as noted in Section 2, large kurtosis values are driven in part by the presence of a 'peaky' MDF, but more importantly, the impact of extended 'heavy' tails. These tails (positive or negative) are driven by the coordinated AMRs and are reflected in the generally large values of kurtosis relative to the Milky Way's distribution.

Alongside the skewness and kurtosis determinations, we present four measures of the shape of the MDF, through its dispersion, or width, at different amplitudes. This is done via the width of the IQR, IDR, ICR and ITPR.[17]

The metrics associated with these width measures require some comment in relation to the information provided by Fig. 3. Specifically, the best-fitting single Gaussian fits overlaid in each panel show that grossly speaking, the Milky Way's and Fornax's MDF are broader than those associated with the simulations.[18] At first glance, the IQR, ITR, etc., measures listed in Table 2 appear counter to this result (which are all, essentially, larger than the values found for GCScut, for example). It is important to remember though that, much like the case for skewness and kurtosis, these measures of the breadth of the MDF are sensitive to the impact of outliers in the tails of the distribution.

It is particularly useful to note the quantitative impact of the role of metal diffusion in setting the width of the MDF in tails of the distribution. For example, in the solar neighbourhood of the Milky Way, the range in metallicity between the bottom and top 0.1 per cent of the stars is ∼2 dex. For our simulation in which metal diffusion was neglected (11mNoDiff), the corresponding width is ∼5 dex – i.e. a factor of ∼1000 times greater than the other simulations with
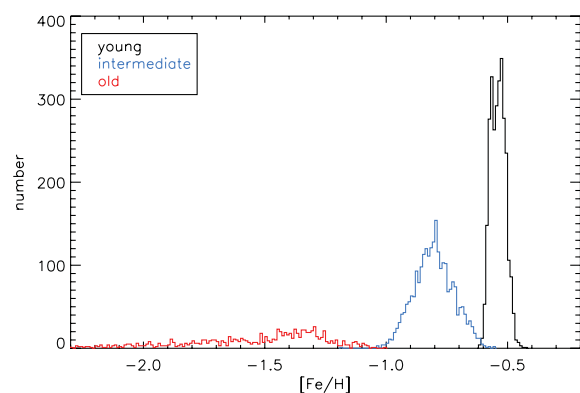

Figure 4. The [Fe/H] MDF in the 'solar neighbourhood' of 11mKroupa, split into three age intervals: young (black) defined as any star particle in the solar neighbourhood at redshift $z = 0$ with an age less than 1 Gyr; intermediate (blue) defined as any star with an age between 5 and 7 Gyr and old (red) defined as any star with an age greater than 9 Gyr.

diffusion and that encountered in the Milky Way, similar to what we found for other low-diffusion runs (Pilkington et al. 2012a).

After Casagrande et al. (2011), we show in Fig. 4 the MDF for the solar neighbourhood of one of our fiducial simulations (11mKroupa), but now binned more finely in metallicity and colour coded by age. Here, young stars correspond to those formed in the last 1 Gyr at redshift $z = 0$; intermediate-age stars are those with ages between 5 and 7 Gyr; old corresponds to stars with ages greater than 9 Gyr. Using the GCS, Casagrande et al. (2011) conclude that the younger stars have a narrower MDF than the older stars, consistent with our results (and to be expected, given its AMR). Casagrande et al. (2011) also found though that the locations of the peaks associated with these old and young stars were at the same metallicity, which is not consistent with our simulations. Again, this is to be expected given the tightly correlated AMRs of the simulations, relative to that of the Milky Way.

While it may be the case that we are not capturing all of the relevant stellar migration physics within these simulations (e.g. bars, spiral arms, resonances, etc.), there *is* radial migration occurring. That said, the radial gradients are shallow for these fiducial dwarfs

---

[17] The IQR corresponds to the difference in metallicity between the 25 per cent lowest metallicity stars and the 25 per cent higher metallicity stars; similarly, the IDR corresponds to the difference between the 10 per cent lowest and 10 per cent highest metallicity stars, etc.
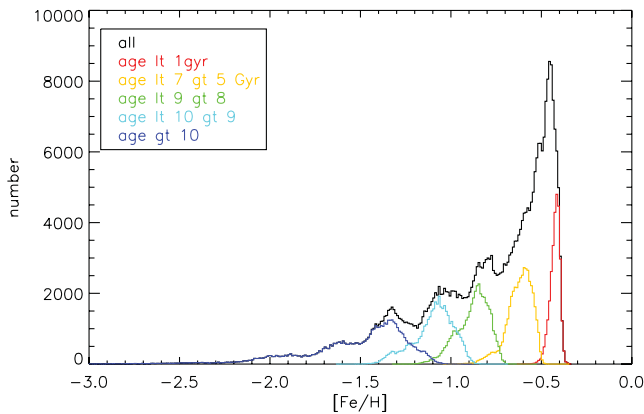
[18] Save for 11mNoDiff, as noted in Section 3.

Figure 5. The [Fe/H] MDF of the 'bulge' of `11mKroupa`; here, the bulge is simply defined as those stars located within 2 kpc of the galactic centre at $z = 0$. Alongside the full MDF (black line), subcomponents based upon the age intervals noted in the inset are overdrawn.

$(-0.01$ to -0.02 dex kpc^{-1}, recalling Table 1[19]) and, as such, over the few kpc of 'disc' associated with each simulated dwarf, systematic migration of metal-rich inner-disc stars outwards (and vice versa) has little impact on the position of the MDF 'substructure' (in which the young, intermediate and old 'peaks' are offset by $\sim 0.3-0.5$ dex from one another). Again, this is entirely consistent with the expected behaviour, based upon the AMR (Fig. 2).

The central regions of our simulations show similar characteristics to those seen in the simulated solar neighbourhoods. Specifically, the [Fe/H] MDF of the 'bulge' (inner 2 kpc) shows a peak near [Fe/H] ~ -0.5, with a number of subcomponents at lower metallicity which correspond to progressively older and metal-poor populations (see Fig. 5). In spirit, such behaviour has been seen in the MDF of the bulge of the Milky Way, where Bensby et al. (2011) find two populations, also separated comparably in age and metallicity, with which they associate separate formation scenarios. Similarly, Hill et al. (2011) find bulge subcomponents within the MDF which they also separate into separate age, metallicity and kinematic substructures, concluding that the metal-poor component can be associated with an old spheroid and the more metal-rich component can be associated with a longer time-scale event (perhaps the evolution of the bar/psudeo-bulge). In our simulations, we see systematic trends in age and kinematics for each metallicity subcomponent of Fig. 5, in the sense of the more metal-poor components being older and progressively less rotationally supported, in exactly the manner one might predict from the AMR (Section 3). It should be emphasized though that within the simulations, the behaviour of these age, metallicity and kinematic 'substructure' in the bulge MDF is continuous, rather than showing any discrete transition from rotational support to anisotropic velocity support.

Finally, we now examine in slightly more detail the behaviour of the extreme metal-poor tails of the simulated MDFs (see Figs 6 and 7). In Fig. 6, we show all stars beyond the inner 3 kpc (and within 10 kpc), in order to minimize the effect of the 'spheroid' stars in the analysis. We experimented, as before, with the impact of using a full kinematic decomposition between disc and spheroid stars, but again, for these dwarfs, the spatial cut alone is indistinguishable from the

[19] Flatter than the gradients seen in our work on the massive galactic analogues to these dwarfs (Pilkington et al. 2012b), consistent with the empirical work on gradients in dwarfs (e.g. Carrera et al. 2008).
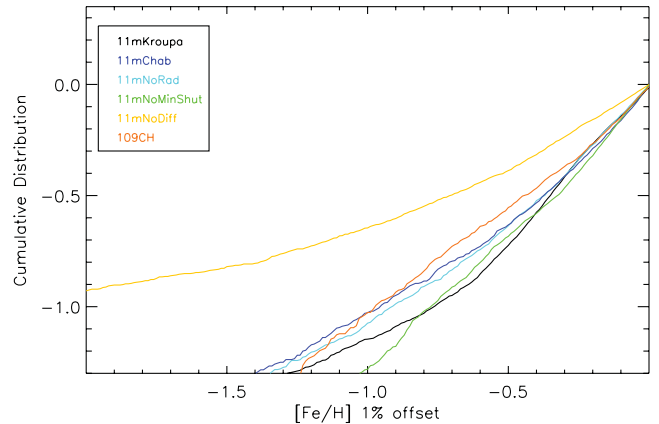

Figure 6. The cumulative MDFs of the five `11m` simulations: `11mKroupa` (black), `11mNoRad` (cyan), `11mChab` (blue), `11mNoMinShut` (green) and `11mNoDiff` (gold), in addition to that of `109CH` (orange: Sánchez-Blázquez et al. (2009)). For these six simulations, all stars lying within 3 and 10 kpc of their respective galactic centres are included in the analysis. The normalization in each case is at the metallicity corresponding to that of the lowest 1 per cent (in terms of [Fe/H]) of the stars in each case.
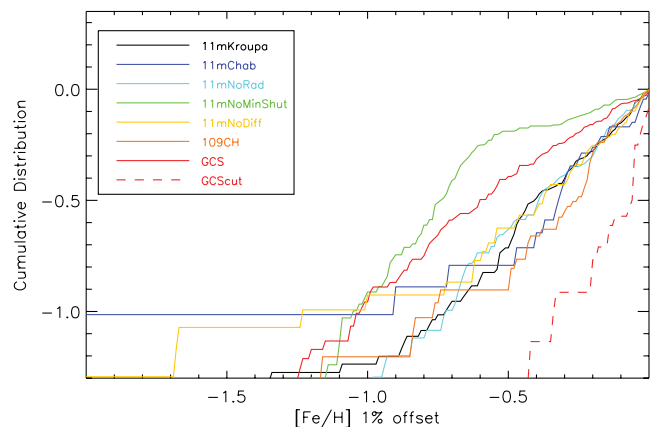

Figure 7. The cumulative MDFs of the analogous solar neighbourhoods associated the five `11m` simulations: `11mKroupa` (black), `11mNoRad` (purple), `11mChab` (blue), `11mNoMinShut` (green) and `11mNoDiff` (gold), in addition to that of `109CH` (orange: Sánchez-Blázquez et al. (2009)). For these six simulations, the solar neighbourhood is defined spatially to include stars lying between 3 and 3.5 disc scalelengths from their respective galactic centres, and within 0.5 kpc of the mid-plane. The `GCS` and `GCScut` subsamples described in Section 2 are shown in red. The normalization for each curve is as described for Fig. 6.

decomposed galaxy. In Fig. 7, we only show those star particles lying within the previously defined 'solar neighbourhoods' of each simulation.

One additional curve is included in both figures (labelled '`109CH`'), that of the disc generated with the adaptive mesh refinement code RAMSES and described by Sánchez-Blázquez et al. (2009), in which diffusion is handled 'naturally'. As noted previously, each of the `11m` series of simulations employs the Shen et al. (2010) metal diffusion framework with a diffusion coefficient $C = 0.05$, except for (obviously) `11mNoDiff` which assumes $C = 0.0$.

Each of the cumulative MDFs (Figs 6 and 7) is normalized. In both cases, the normalization occurs at [Fe/H] corresponding to the metallicity of the lowest 1 per cent of the stars (in terms of [Fe/H]). For plotting purposes, these are then aligned arbitrarily at

[Fe/H] $\equiv +0.0$, to show the relative distributions of extremely low-metallicity stars within each simulation and the empirical data sets. One could take a different approach and, say, normalize at (i) the same metallicity, (ii) the same amplitude or (iii) the same number of stars. For example, in our analysis of the Governato et al. (2010) bulgeless dwarf galaxy simulations (Pilkington et al. 2012a), we adopted (i), normalizing all MDFs at [Fe/H] = −2.3. This was similar in spirit to Schörck et al. (2009), who fixed the normalizations of the Milky Way halo and Local Group dwarf spheroidal MDFs to be unity at the metallicity corresponding to the lowest (in terms of [Fe/H]) ∼100 stars in each. For distributions which peak at (potentially) very different metallicities, such normalizations can result in significant outliers which are not necessarily driven by any MDF 'tail'.[20] For our work here, while small quantitative differences exist depending upon the adopted normalization, the qualitative results are robust regardless of the choice.

What is immediately clear from even a cursory examination of Fig. 6 is that the relative distribution of extremely metal-poor stars within all the simulations in which metal diffusion acts – i.e. all but `11mNoDiff` – are consistent with each other. This reflects graphically what we have commented upon earlier in relation to the tabulated ICR and ITPR values for the various MDFs (Table 2). Specifically, the lack of metal diffusion within `11mNoDiff` drives its discrepant ICR and ITPR values (Table 2), and its outlier status in Fig. 6. When compared with fig. 5 of Pilkington et al. (2012a), one can see that the overly 'heavy' metal-poor tail to the MDF of `11mNoDiff` matches that encountered in, for example, the low-metal-diffusion simulations of Governato et al. (2010).[21] One fairly robust conclusion that can be drawn from Fig. 6 is that the *relative* distribution of *extremely* metal-poor stars is robust against the choice of feedback scheme; instead, diffusion plays a more important role in shaping this distribution.

In some sense, the better 'statistics' afforded by Fig. 6 provides a 'cleaner' picture than that seen when restricting the analysis to just the 'solar neighbourhoods'.[22] For completeness though, in Fig. 7 we also show the cumulative MDFs of the metal-poor tails for each data set, normalized as in Fig. 6. We should emphasize though that the small number of star particles in the 'bottom' 1 per cent (in terms of metallicity) of the `11mNoDiff`, `11mChab` and `GCScut` samples (∼30 in each) make any interpretation susceptible to small-number statistics (and stochastic point-to-point 'fluctuations' which are 'averaged' over when employed the full disc, as in Fig. 6).

5 SUMMARY

Employing a suite of five simulations of an M33-scale late-type disc galaxy, each with the same assembly history, but with different prescriptions for stellar and SNe feedback, IMFs, metal diffusion and SN remnant cooling 'shut-off' period, we have analysed the resulting chemistry of the stellar populations, with a particular focus on the MDFs and the characteristics of the extreme metal-poor tail of said distributions.

In the context of the distribution of metals (in the sense of the higher order moments of the resulting MDFs) within these discs,

the impact of feedback and the IMF is more subtle than that of, for example, metal diffusion. Employing a Chabrier (2003) IMF, rather than the Kroupa et al. (1993) form adopted in our earlier work, does impact significantly on the resulting SFH (and associated, reduced, stellar mass fraction, resulting in remarkably close adherence to a wide range of empirical scaling relations – Brook et al. 2011b).

The SFHs of the 'solar' neighbourhoods associated with each simulation show exceedingly tight AMRs. In shape, these relations are akin to those predicted by classical galactic chemical evolution models (e.g. Chiappini et al. 2001; Fenner & Gibson 2003), but bear somewhat less resemblance to that seen, for example, in the Milky Way's solar neighbourhood (Holmberg et al. 2009). These correlated AMRs result inexorably in (negatively) skewed MDFs with large kurtosis values, when compared with the Milky Way. SFHs of dwarf irregulars, which qualitatively speaking are a better match to those of the `11m` series of simulations presented here, suggest though that somewhat steeper AMRs might eventuate in nature in these environments (e.g. Dolphin et al. 2003; Skillman et al. 2003). MDFs and AMRs of a comparable quality to that of the GCS (Holmberg et al. 2009) will be required to substantively progress the field.

An excess 'tail' of extremely metal-poor stars (amongst the bottom 0.1–1 per cent of the most metal-poor stars) – ∼2–3 dex below the peak of the MDF – exists in all of the simulations, as reflected in their ICR and ITPR measures. This tail is particularly problematic in simulations without metal diffusion (`11mNoDiff`) and those for which the diffusion coefficient was set relatively low (e.g. Governato et al. 2010; Pilkington et al. 2012a). As demonstrated, the ICR and ITPR, in the absence of metal diffusion, can be ∼30–3000 times larger than that encountered in the Milky Way.

We end with a restatement of our initial caveat. The simulations presented here (particularly the fiducials, `11mKroupa` and `11mChab`) have been shown to be remarkably consistent with a wide range of scaling relations (Brook et al. 2012b). That said, their SFHs are more akin to those of NGC 6822, Sextans A, WLM, and to some extent, the LMC (at least in the case of `11mChab`) – i.e. these systems are not 'clones' of the Milky Way. We have used the wonderful GCS's wealth of data to generate empirical AMRs and MDFs against which to compare, but exact one-to-one matches are not to be expected. That said, they do provide useful, hopefully generic, relations against which to compare. In the future, we hope to extend our analysis to equally comprehensive data sets for the LMC, making use of, for example, the data provided by the Vista Magellanic Cloud Survey (Cioni et al. 2011).

---

[20] In the case of the analysis of Schörck et al. (2009), the similarity of the positions of the peaks of the Milky Way halo and Local Group dSph MDFs meant that their analysis was robust against the choice of normalization.

[21] Demonstrating the quantitative power of the MDF to constrain the magnitude of diffusion within SPH simulations of galaxy formation.

[22] Given the lack of any substantial gradient in the stellar populations for these dwarfs, the comparison is not invalid.

REFERENCES

Abadi M. G., Navarro J. F., Steinmetz M., Eke V. R., 2003, ApJ, 597, 21

Asplund M., Grevesse N., Sauval A. J., Scott P., 2009, ARA&A, 47, 481

Bensby T. et al., 2011, A&A, 533, A134

Brook C. B., Stinson G., Gibson B. K., Roškar R., Wadsley J., Quinn T., 2012a, MNRAS, 419, 771

Brook C., Stinson G., Gibson B., Wadsley J., Quinn T., 2012b, MNRAS, (arXiv:1201.3359)

Caimmi R., 2008, New Astron., 13, 314

Calura F. et al., 2012, MNRAS, (arXiv:1204.1051)

Carrera R., Gallart C., Aparicio A., Costa E., Méndez R. A., Noël N. E. D., 2008, AJ, 136, 1039

Casagrande L., Schönrich R., Asplund M., Cassisi S., Ramírez I., Meléndez J., Bensby T., Feltzing S., 2011, A&A, 530, A138

Chabrier G., 2003, PASP, 115, 763

Chiappini C., Matteucci F., Romano D., 2001, ApJ, 554, 1044

Cioni M.-R. L. et al., 2011, A&A, 527, A116

Dolphin A. E. et al., 2003, AJ, 126, 187

Dolphin A. E., Weisz D. R., Skillman E. D., Holtzman J. A., 2005, in valls-Gabuad D., Chavez M., eds, ASP Conf. Ser. preprint (astro-ph/0506430)

Fenner Y., Gibson B. K., 2003, PASA, 20, 189

Gibson B. K., 1994, J. R. Astron. Soc. Canada, 88, 383

Gibson B. K., Giroux M. L., Penton S. V., Stocke J. T., Shull J. M., Tumlinson J., 2001, AJ, 122, 3280

Governato F. et al., 2010, Nat, 463, 203

Haardt F., Madau P., 1996, ApJ, 461, 20

Hartwick F. D. A., 1976, ApJ, 209, 418

Haywood M., 2001, MNRAS, 325, 1365

Hill V. et al., 2011, A&A, 534, A80

Holmberg J., Nordström B., Andersen J., 2007, A&A, 475, 519

Holmberg J., Nordström B., Andersen J., 2009, A&A, 501, 941

Holtzman J. A. et al., 1999, AJ, 118, 2262

Hopkins P. F., Quataert E., Murray N., 2011, MNRAS, 417, 950

Kannan R., Macciò A. V., Pasquali A., Moster B. P., Walter F., 2012, ApJ, 746, 10

Kirby E. N., Lanfranchi G. A., Simon J. D., Cohen J. G., Guhathakurta P., 2011, ApJ, 727, 78

Kobayashi C., Nakasato N., 2011, ApJ, 729, 16

Kotoneva E., Flynn C., Chiappini C., Matteucci F., 2002, MNRAS, 336, 879

Kroupa P., Tout C. A., Gilmore G., 1993, MNRAS, 262, 545

Macciò A. V., Stinson G., Brook C. B., Wadsley J., Couchman H. M. P., Shen S., Gibson B. K., Quinn T., 2012, ApJ, 744, L9

McClure-Griffiths N. M., Ford A., Pisano D. J., Gibson B. K., Staveley-Smith L., Calabretta M. R., Dedes L., Kalberla P. M. W., 2006, ApJ, 638, 196

Mollá M., Díaz A. I., 2005, MNRAS, 358, 521

Nordström B. et al., 2004, A&A, 418, 989

Pagel B. E. J., Patchett B. E., 1975, MNRAS, 172, 13

Pilkington K., Gibson B. K., Calura F., Stinson G. S., Brook C. B., Brooks A., 2012a, in Recchi S., Hensler G., Papaderos P., eds, JENAM 2010, Joint European and National Astronomy Meeting: The Chemical and Dynamical Evolution of Isolated Dwarf Galaxies. Springer, Berlin, p.47

Pilkington K. et al., 2012b, A&A, 540, A56

Raiteri C. M., Villata M., Navarro J. F., 1996, Mem. Soc. Astron. Ital., 67, 817

Renda A., Kawata D., Fenner Y., Gibson B. K., 2005, MNRAS, 356, 1071

Robertson B. E., Kravtsov A. V., 2008, ApJ, 680, 1083

Roškar R., Debattista V. P., Quinn T. R., Stinson G. S., Wadsley J., 2008, ApJ, 684, L79

Sánchez-Blázquez P., Courty S., Gibson B. K., Brook C. B., 2009, MNRAS, 398, 591

Schlesinger K. J. et al., 2012, preprint (arXiv:1112.2214)

Schoenrich R., Binney J., 2008, MNRAS, 396, 203

Schörck T., Christlieb N., Cohen J. G., Beers T. C., Shectman S., Thompson I., 2009, A&A, 507, 817

Shen S., Wadsley J., Stinson G., 2010, MNRAS, 407, 1043

Skillman E. D., Tolstoy E., Cole A. A., Dolphin A. E., Saha A., Gallagher J. S., Dohm-Palmer R. C., Mateo M., 2003, ApJ, 596, 253

Sommer-Larsen J., Fynbo J. P. U., 2008, MNRAS, 385, 3

Springel V. et al., 2008, MNRAS, 391, 1685

Stinson G., Seth A., Katz N., Wadsley J., Governato F., Quinn T., 2006, MNRAS, 373, 1074

Stinson G. S., Bailin J., Couchman H., Wadsley J., Shen S., Nickerson S., Brook C., Quinn T., 2010, MNRAS, 408, 812

Stinson G. et al., 2012, preprint (arXiv:1112.1698)

Tinsley B. M., 1980, Fundamentals Cosmic Phys., 5, 287

Tissera P. B., White S. D. M., Scannapieco C., 2011, MNRAS, 420, 255

Tumlinson J. et al., 2011, Sci, 334, 948

van den Hoek L. B., Groenewegen M. A. T., 1997, A&AS, 123, 305

Vera-Ciro C. A., Helmi A., Starkenburg E., Breddels M. A., 2012, (arXiv:1202.6061)

Wadsley J. W., Stadel J., Quinn T., 2004, New Astron., 9, 137

Wiersma R. P. C., Schaye J., Theuns T., 2011, MNRAS, 415, 353

Woosley S. E., Weaver T. A., 1995, ApJS, 101, 181

This paper has been typeset from a TeX/LaTeX file prepared by the author.